

Nebular H α emission in SN Ia 2016jae

N. Elias-Rosa^{1,2}, P. Chen³, S. Benetti¹, Subo Dong³, J. L. Prieto^{4,5}, E. Cappellaro¹, J. A. Kollmeier⁶, N. Morrell⁷,
A. L. Piro⁶, and M. M. Phillips⁷

¹ INAF – Osservatorio Astronomico di Padova, vicolo dell’Osservatorio 5, Padova 35122, Italy
e-mail: nancy.elias@inaf.it

² Institute of Space Sciences (ICE, CSIC), Campus UAB, Carrer de Can Magrans s/n, 08193 Barcelona, Spain

³ Kavli Institute for Astronomy and Astrophysics, Peking University, Yi He Yuan Road 5, Hai Dian District, Beijing 100871, China

⁴ Núcleo de Astronomía de la Facultad de Ingeniería y Ciencias, Universidad Diego Portales, Av. Ejército 441, Santiago, Chile

⁵ Millennium Institute of Astrophysics, Santiago, Chile

⁶ Observatories of the Carnegie Institution for Science, 813 Santa Barbara Street, Pasadena, CA 91101, USA

⁷ Las Campanas Observatory, Carnegie Observatories, Casilla 601, La Serena, Chile

Received XXXX; accepted XXXX

ABSTRACT

There is a wide consensus that type Ia supernovae (SN Ia) originate from the thermonuclear explosion of CO white dwarfs (WD), with the lack of hydrogen in the observed spectra as a distinctive feature. Here, we present SN 2016jae, which was classified as a Type Ia SN from a spectrum obtained soon after the discovery. The SN reached a B-band peak of -17.93 ± 0.34 mag, followed by a fast luminosity decline with s_{BV} 0.56 ± 0.06 and inferred $\Delta m_{15}(B)$ of 1.88 ± 0.10 mag. Overall, the SN appears as a “transitional” event between “normal” SNe Ia and very dim SNe Ia such as 91bg-like SNe. Its peculiarity is that two late-time spectra taken at +84 and +142 days after the peak show a narrow line of H α (with full width at half-maximum of ~ 650 and 1000 km s $^{-1}$, respectively). This is the third low-luminosity and fast-declining Type Ia SN after SN2018cqj/ATLAS18qtd and SN2018fhw/ASASSN-18tb, found in the 100IAS survey that shows resolved narrow H α line in emission in their nebular-phase spectra. We argue that the nebular H α emission originates in an expanding hydrogen-rich shell (with velocity ≤ 1000 km s $^{-1}$). The hydrogen shell velocity is too high to be produced during a common envelope phase, while it may be consistent with some material stripped from an H-rich companion star in a single-degenerate progenitor system. However, the derived mass of this stripped hydrogen is ~ 0.002 - 0.003 M $_{\odot}$, which is much less than that expected (>0.1 M $_{\odot}$) for standard models for these scenarios. Another plausible sequence of events is a weak SN ejecta interaction with a H-shell ejected by optically thick winds or a nova-like eruption on the C/O WD progenitor some years before the supernova explosion.

Key words. supernovae: general; supernovae: individual: SN 2016jae; supernovae: individual: SN 2018cqj; supernovae: individual: SN 2018fhw

1. Introduction

Type Ia supernovae (SN Ia) are believed to originate from the thermonuclear explosion of CO white dwarfs (WD). In a popular explosion scenario, the WD is in a close binary system with another WD (double degenerate system), or with a non-degenerate mass-donor companion, either a main sequence, or a giant star (single degenerate system). In the merging scenario, the combined mass of the WDs may meet or exceed the Chandrasekhar limit (~ 1.4 M $_{\odot}$), while in the single degenerate, the mass transfer from the secondary star makes the primary WD approaches the Chandrasekhar limit. In both cases, the final fate of the system is the explosion. There are also alternative scenarios in which the explosion occurs without reaching the Chandrasekhar mass (i.e., a sub-Chandrasekhar-mass explosion). Which is the dominant scenario is still unknown (see, e.g., Maoz et al. 2014). A distinctive feature of SNe Ia is the lack of hydrogen in the observed spectra. Yet, at least for single degenerate systems, it is expected that some H from the main-sequence companion star is left in the system. In fact, finding H in SNe Ia would strongly support the single degenerate scenario. Several attempts have been made to detect H in SNe Ia, but no convincing evidence has been found yet (e.g. Mattila et al. 2005; Tucker et al. 2020). Hydrogen has been found so far only in the SNe Ia-CSM (circum-

stellar material) events, where narrow H emissions are present since early phases and probably excited in the shock between the SN ejecta and H-rich CSM (e.g. Hamuy et al. 2003; Prieto et al. 2007; Dilday et al. 2012; Silverman et al. 2013; consider also Benetti et al. 2006 for an alternative interpretation).

Recently, two cases have been reported of low-luminosity SNe Ia with detection of narrow H α emission lines in late-time spectra: SN 2018fhw/ASASSN-18tb (Kollmeier et al. 2019; Valley et al. 2019) and SN 2018cqj/ATLAS18qtd (Prieto et al. 2020). These two SNe were followed as part of the 100IAS survey (Dong et al. 2018), a project aiming at collecting a homogeneous sample of ~ 100 SNe Ia with optical nebular-phase spectra using 5-10 meter class telescopes. Both SNe show strong emission lines of H α at phases > 100 d, with luminosities in the range of $\sim 10^{36}$ - 10^{38} erg s $^{-1}$ (H α emission lines in SNe Ia-CSM can reach luminosities in the range 10^{40} - 10^{41} erg s $^{-1}$; Silverman et al. 2013).

Here we report a third case, SN 2016jae ($\alpha = 09^{\text{h}} 42^{\text{m}} 34^{\text{s}}.49$, $\delta = +10^{\circ} 59' 35''.7$; J2000.0), also known as ATLAS16eay, MASTER OT J094234.49+105935.7, CSS170201-094234+105935, Gaia16cev and PS16fkf. It was discovered on 2016 December 21.99 UT, with an unfiltered magnitude of 17.2, by the MASTER Global Robotic Net (Gress et al.

2016)¹. Independent discoveries were also reported by the Asteroid Terrestrial-impact Last Alert System (ATLAS, Tonry et al. 2018, Smith et al. 2020; Tonry et al. 2016), Gaia transient survey (Hodgkin et al. 2013) and Pan-STARRS (Chambers et al. 2016, Magnier et al. 2020). It was classified on 2016 December 28.34 UT (Smith et al. 2016b,a) as a Type Ia SN approximately one week post-maximum, by the Public ESO -European Southern Observatory- Spectroscopic Survey for Transient Objects (PESSTO; Smartt et al. 2015).

In the next section (Section 2), we describe the host environment of SN 2016jae. Photometric and spectroscopic data are analysed in Section 3. And the discussion is in Section 4.

2. Host environment

The galaxy in the closest angular separation with SN 2016jae is SDSS J094234.46+105931.1 (hereafter SDSS-SW), a tiny galaxy located at 4′.2 S, 0′.6 W from the SN (see Fig. 1). The candidate host galaxy has a magnitude in *r* of 21.67 and a photometric redshift of 0.35 ± 0.08 according to the Sloan Digital Sky Survey (SDSS) DR15 catalogue². However, the redshift derived from the spectrum of SN 2016jae using the Supernova Identification cross-correlation code (SNID; Blondin & Tonry 2007), $z = 0.021 \pm 0.006$, is not consistent with the redshift of that galaxy.

There are other two galaxies in the proximity of SN 2016jae, SDSS J094235.65+105905.3 (hereafter SDSS-SE), and SDSS J094234.01+110022.8 (hereafter SDSS-NW) located at 30′.0 S, 17′.3 E and 47′.5 N, 7′.3 W, respectively, from the SN. We took a spectrum of SDSS-SW and SDSS-SE with the 10 m Gran Telescopio Canarias (GTC) on 2019 December 3, and another spectrum of SDSS-SW and SDSS-NW always with GTC on 2020 May 10. Both spectra were reduced as described in Section 3.2. In the case of SDSS-SW, we combine the spectra of different epochs to improve the signal-to-noise ratio (see Fig. A.1). Comparing the spectrum of SDSS-SW with a template spectrum of a late-type galaxy (from the Kinney-Calzetti Spectral Atlas; Calzetti et al. 1994; Kinney et al. 1996) and measuring the position of H α , H β , [O II] and [O III] emission lines, we found that SDSS-SW is consistent with being a background galaxy at $z=0.285 \pm 0.009$ (similarly to the SDSS photometric redshift). Measuring the position of the same emission lines, plus [N II] and [S II] in the SDSS-SE spectrum, and H α , [O III] and [S II] in SDSS-NW, we derive a redshift of 0.021 ± 0.001 and 0.019 ± 0.001 , respectively, which are consistent with the redshift of the SN derived from fitting its near-peak spectrum. This suggests that SN 2016jae exploded in the outer halo of one of these galaxies, most likely in SDSS-SE for being the closest one. Throughout the paper, we adopt $z_{\text{host}} = 0.021$ of SDSS-SE as the reference redshift. However, we cannot rule out that the SN is actually located in the halo of SDSS-NW. The implication assuming $z_{\text{host}} = 0.019$ is discussed in Sect. 4. From the adopted redshift we derived a luminosity distance of 92.9 ± 4.3 Mpc³ ($m-M = 34.8 \pm 0.1$ mag), assuming a Hubble constant $H_0 = 67.8$ km s⁻¹ Mpc, $\Omega_m = 0.31$ and $\Omega_\Lambda = 0.69$ (Planck Collaboration et al. 2016). With this distance, the projected linear offset from the SDSS-SE nucleus is 15.6 kpc.

The Milky Way extinction along the line of sight of the supernova is $A_{V,\text{MW}} = 0.051$ mag (NED⁴; Schlafly & Finkbeiner 2011). There is no evidence of narrow Na I D absorption in the spectra, which would indicate the presence of gas/dust on the line of sight. Taking advantage of the fact that SNe Ia are known for their “homogeneity”, we considered different methods to estimate the extinction (A_V) toward SN 2016jae based on comparisons of the object’s spectral energy distribution (SED) and luminosity with those of other similar SNe Ia. As we will discuss in the next section, SN 2016jae is a transitional event between “normal” SNe Ia and sub-luminous SNe Ia such as SN 1991bg. Then, we matched the intrinsic $(B-V)_0$, and $(r-i)_0$ colour curves of SN 2016jae with those of SN 2018cqj (Prieto et al. 2020), SN 2018fhw (Vallely et al. 2019) (which have a similar decline rate), and SN 1991bg, the prototype of sub-luminous SNe Ia (Filippenko et al. 1992; Leibundgut et al. 1993; Turatto et al. 1996), obtaining $E(B-V)_{V,\text{tot}} = 0.09 \pm 0.03$ mag (see Figure A.2). For comparison we also show the colour curves of the “normal” Type Ia SNe 1992A (Kirshner et al. 1993) and 2011fe (Pereira et al. 2013). Besides, we contrasted the early-time optical SED of SN 2016jae with those of 91bg-like SNe Ia at similar epoch. The SED of the reference SNe were first corrected for redshift and Galactic extinction. From this comparison a colour excess of $E(B-V)_{V,\text{host}} = 0.09 \pm 0.01$ mag was derived. We adopt $E(B-V) = 0.10 \pm 0.03$ mag, i.e., $A_V = 0.30 \pm 0.10$ mag, as the total extinction toward SN 2016jae.

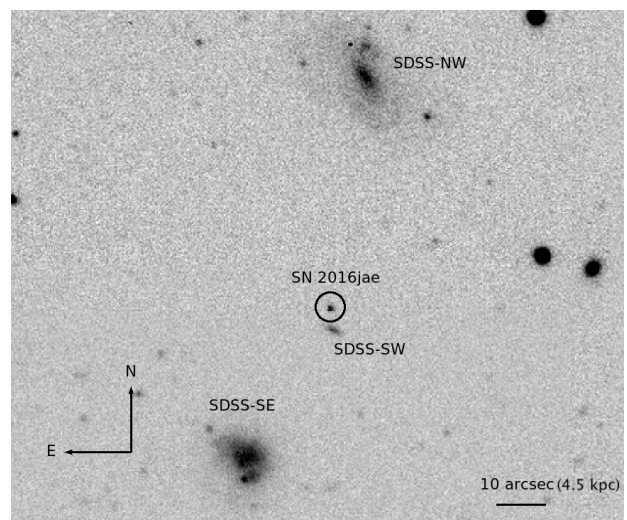


Fig. 1. DECaLS DR7 *r* deep image of the SN 2016jae field. The SN and the three nearby galaxies discussed in the text (SDSS-SW, SDSS-SE, and SDSS-NW) are indicated. We consider $D_L = 92.9 \pm 4.3$ Mpc to estimate the physical projected distance in the scale bar. We argue that SN 2016jae exploded most likely in the outer halo of SDSS-SE, as this is the nearest galaxy with a similar redshift.

3. Data and analysis

3.1. Photometry

We used *BVri* photometry of SN 2016jae between 2016 December 28 (close to its peak magnitude) and 2017 February 13 from

¹ <http://master.sai.msu.ru/en/>

² <http://skyserver.sdss.org/dr15/en/home.aspx>

³ An uncertainty of the velocity of 250 km s⁻¹ was added in quadrature to the distance error (see, Burns et al. 2018).

⁴ The NASA/IPAC Extragalactic Database (NED) is funded by the National Aeronautics and Space Administration and operated by the California Institute of Technology.

the CNIA0.02 programme⁵ (Chen et al. 2020) and taken with the 1 m telescopes at the Las Cumbres Observatory Global Telescope Network (LCOGT; Brown et al. 2013). We also retrieved three epochs of *gaia*-band photometry from the Gaia transient survey⁶, and a late-time (phase 142d) *r*-band photometric measurement of SN 2016jaj with the 10.4 m GTC+OSIRIS at the Roque de los Muchachos Observatory (Spain). The Gaia data were converted to *r*-band magnitude using the relationships reported in Gaia Data Release 2 Documentation (release 1.2)⁷. GTC SN magnitudes were measured using Point-Spread-Function (PSF) fitting with SNOoPy⁸ pipeline. We calibrated the instrumental magnitudes to standard photometric systems, using the zero points and colour terms measured through reference SDSS stars in the field of SN 2016jaj. We present the final calibrated photometry of SN 2016jaj in Table C.1.

The *BVri* light curves of SN 2016jaj are shown in the left panel of Figure 2. The data are relative to the *B* maximum date occurring on 2016 December 28.2, or MJD 57750.2 \pm 1.0. It was obtained by matching the light curves peak with the SNOoPy fitting package (Burns et al. 2011) using the colour stretch parameter s_{BV} models. Allowing for the poor sampling around the maximum light, we obtained the following fits: $B_{max} = 17.32 \pm 0.11$ mag, $V_{max} = 16.77 \pm 0.07$ mag, $r_{max} = 16.78 \pm 0.07$ mag, $i_{max} = 17.07 \pm 0.08$ mag and $s_{BV} = 0.56 \pm 0.06$. The light curves of SN 2016jaj have a good sampling after maximum light up to +42 d later, showing in all bands a fast decline until the radioactive decay at $t \sim 20$ d in *B*-band. The latter translates to $\Delta m_{15}(B)$ of 1.88 ± 0.10 mag using the s_{BV} - Δm_{15} relationship in Burns et al. (2018). Based on the light curves, SN 2016jaj qualifies as an intermediate case between “normal” and sub-luminous and fast-declining Type Ia supernovae. In fact,

- The Δm_{15} of SN 2016jaj is between that typical for “normal” SNe Ia, $\lesssim 1.7$ mag, and that of 91bg-like SNe, 1.8-2.1 mag (see, e.g., Taubenberger 2017).
- The *B* absolute magnitude peak of SN 2016jaj is -17.93 ± 0.34 , dimmer than “normal” Type Ia SNe such as SNe 1992A and 2011fe (see Figure 2, right panel) and similar to other fast-decliner objects such as SNe 2018cqj and 2018fhw. We note that the latter SNe are more luminous than SN 1991bg, as illustrated in Figure 2. Indeed, the location of SN 2016jaj in the figure $M_{B_{max}}$ vs. $(B_{max} - V_{max})$ colour (figure 7 of Phillips 2012) falls rather close to transitional supernovae such as the 86G-like (see Fig. A.3).
- The “pseudo-bolometric” (integrating the flux in the *BVri* bands) peak luminosity of SN 2016jaj, $\log(L) = 42.49 \pm 0.07$ is consistent with those of other sub-luminous Type Ia supernovae.
- Differently from 91bg-like SNe, the light curve in *i*-band shows a flattening at ~ 20 days, yet not a secondary peak as typically seen in the redder light curves of “normal” SNe Ia. According to Kasen 2006 and Blondin et al. 2015, the secondary near-infrared peak in SNe Ia is related to a recombination wave propagating through chemically stratified ejecta.

Consequently, the recombination of Fe III to Fe II would occur earlier in less luminous and cooler SNe.

- We can estimate the mass of ^{56}Ni synthesized in an explosion through the bolometric peak (Stritzinger & Leibundgut 2005). We derived a lower limit (because we have integrated only the flux in the *BVri* bands) for the ^{56}Ni mass of $0.15 M_{\odot}$ for SN 2016jaj. Similar masses have been also estimated for SNe 2018cqj and 2018fhw⁹ (computed in a similar manner). This is marginally larger than the range found for the 91bg-like SNe (between 0.05 and $0.10 M_{\odot}$; Taubenberger 2017).

3.2. Spectroscopy

We analyze three optical spectra of SN 2016jaj (see Table C.2 for basic information on the spectroscopic observations). The first spectrum was taken for the transient classification at the 3.6m New Technology Telescope (NTT) on 2016 December 28.34 by the international collaboration PESSTO¹⁰. Two more spectra were obtained at nebular phase, on 2017 March 22.19 and 2017 May 18.91, with the Magellan Clay telescope (as part of 100IAS) at Las Campanas Observatory and with GTC at Roque de los Muchachos Observatory, respectively. All the spectra were obtained with the slit aligned with the parallactic angle to minimize differential flux losses caused by atmospheric refraction.

All spectra were reduced following standard procedures with IRAF routines. The two-dimensional frames were corrected by bias and flat-field, before the extraction of the one-dimensional spectra. We wavelength calibrate the spectra by comparison with arc-lamp spectra. The flux calibration was done using spectrophotometric standard stars, which also help for removing the strongest telluric absorption bands present in the spectra (in some cases, residuals are still present after the correction). The wavelength calibration was verified against the bright night-sky emission lines. Finally, the absolute flux calibration of the spectra was cross-checked against the broadband photometry: *BVri* SED at a contemporaneous phase for the first spectrum, *Vri* extrapolated SED for the second spectrum and *r* band for the late time spectrum. In all three cases, we scaled the spectra by a constant value (ranging from 0.8 to 1.9), assuring a final accurate match with the photometry of < 0.15 mag.

Figure 3 shows the three optical spectra of SN 2016jaj. The first spectrum of SN 2016jaj is similar to that of “normal” Type Ia SNe, except for the unusually prominent O I $\lambda 7774$ and Ti II (between 4000 and 4400 Å) features, more common of faster-decliner and sub-luminous SNe Ia such as 91bg-like SNe and transitional events like SN 1986G (Taubenberger 2017; see also panel (a) of Figure A.4). In fact, $\mathcal{R}(\text{Si II})$ (Nugent et al. 1995), the ratio between the strength of the absorptions of Si II $\lambda 5972$ and $\lambda 6355$, is close to that of the FAINT and CL (‘cool’) families according to Benetti et al. (2005) and Branch et al. (2006), respectively¹¹. The late-time spectra of SN 2016jaj also exhibit

⁵ Collection of a Complete, Nearby, and effectively unbiased sample of Type Ia Supernovae at host-galaxy redshifts $z_{\text{host}} < 0.02$.

⁶ <http://gsaweb.ast.cam.ac.uk/alerts>

⁷ https://gea.esac.esa.int/archive/documentation/GDR2/Data_processing/chap_cu5pho/sec_cu5pho_calibr/ssc_cu5pho_PhotTransf.html

⁸ SNOoPy is a package for SN photometry using PSF fitting and/or template subtraction developed by E. Cappellaro. A package description can be found at <http://sngroup.oapd.inaf.it/ecsnoopy.html>.

⁹ Our estimation of ^{56}Ni mass for SN 2018fhw is consistent with the value derived by Valley et al. (2019), $0.2 M_{\odot}$.

¹⁰ The spectrum was taken from WiseREP (Yaron & Gal-Yam 2012); <https://wiserep.weizmann.ac.il>.

¹¹ FAINT SNe Ia (one of the three families grouped by Benetti et al. 2005 according they observed diversities) are characterized by having low expansion velocities and rapid evolution of the Si II velocity. In the classification scheme of Branch et al. (2006), the CL or cool SNe Ia are those with moderate values of pseudo-equivalent width of the Si II $\lambda 6355$ line, but large values of pseudo-equivalent width of the Si II $\lambda 5972$ line.

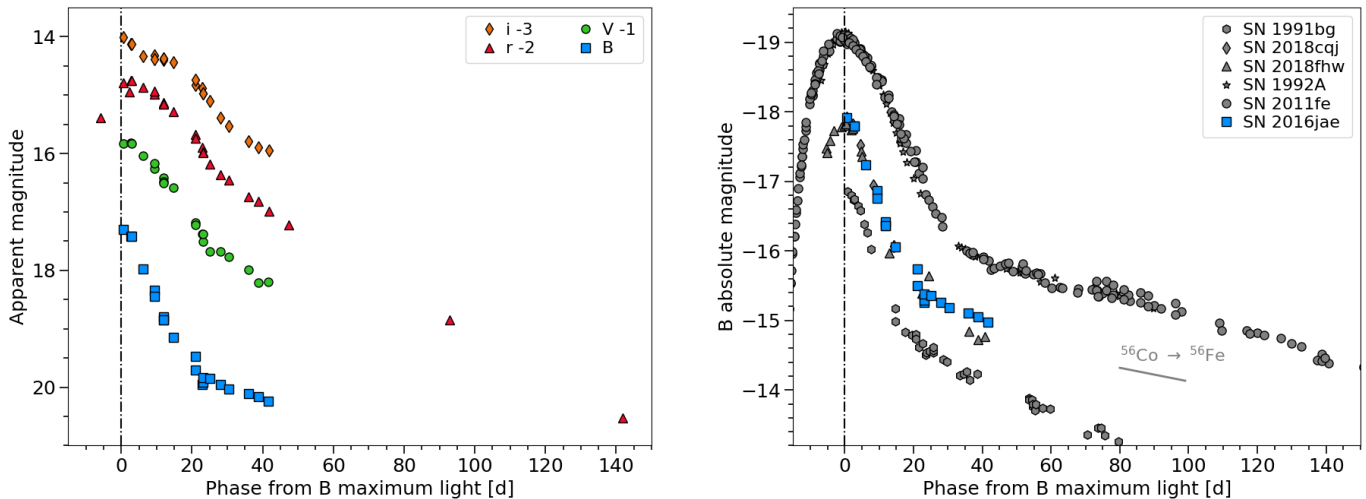


Fig. 2. *Left:* *BVri* light curves of SN 2016jae. The light curves have been shifted for clarity by the amounts indicated in the legend. *Right:* Absolute *B* light curve of SN 2016jae, shown along with those of SNe 1991bg, 2018cuj, 2018fhw, 1992A and 2011fe. For both panels, the dot-dashed vertical line indicates the *B*-band maximum light. The uncertainties for most data points are smaller than the plotted symbols. A colour version of this figure can be found in the online journal.

features previously seen in 91bg-like and transitional SNe Ia. The spectra are dominated by narrow [Fe II], [Fe III] and [Co III], and broad [Ca II]/[Fe II] emission lines (panel (b) of Figure A.4).

Motivated by the two preceding discoveries of nebular H α lines in 100IAS, we inspected the spectra of SN 2016j_{ae} and noticed the presence of a significant H α emission line. It is weak and barely visible at phase 84.0d, but well seen at phase 141.8d (see also the 2D image of the spectrum in Figure 4 and the H α line profile comparison in Figure A.5, which support our belief that the H α line is intrinsic to the SN spectrum and not a contamination from nearby galaxy background). This same line is also present in the nebular spectra of SNe 2018c_{qj} and 2018f_{hw} at similar phases, as can be seen in Figure 5, left panel. The H α line of SN 2016j_{ae} appears on top of a broader feature, probably due to a blend of iron-group elements (see, e.g., Mazzali et al. 1997). We decompose the line profiles into three Gaussian profiles, one for the narrow H α and two components to match the broad iron-peak element feature (see Elias-Rosa et al. 2016 for more details in the procedure). The right panels of Figure 5 show the result of the multi-component fit. The profiles are well reproduced with a narrow component centered at ~ 6568 Å rest frame, with full width at half-maximum (FWHM) of ~ 16 Å (~ 650 km s $^{-1}$; after correction for instrumental resolution¹²) at phase 84.0d, and at ~ 6567 Å, with FWHM of ~ 22 Å (~ 1000 km s $^{-1}$) at phase 141.8d. The integrated luminosity of H α was estimated to be $L(84.0d) = (3.0 \pm 0.8 \times 10^{38} \text{ erg s}^{-1})$, and $L(141.8d) = (1.6 \pm 0.2) \times 10^{38} \text{ erg s}^{-1}$. The best-fit luminosity of the H α line decreases by a factor of ~ 2 between the 84.0 and 141.8 days spectra, however, given the error of the flux measurement in the first epoch we cannot exclude that the flux could remain constant. In the case of SN 2016j_{ae}, as well as in SNe 2018c_{qj} and 2018f_{hw}, the H β is not visible. Following the method introduced by Tucker et al. (2020), we have estimated a 10σ upper limit on the H β flux of the order of $\sim 10^{-17} \text{ erg s}^{-1} \text{ cm}^{-2}$. A similar result was also obtained for SNe 2018c_{qj} and 2018f_{hw}.

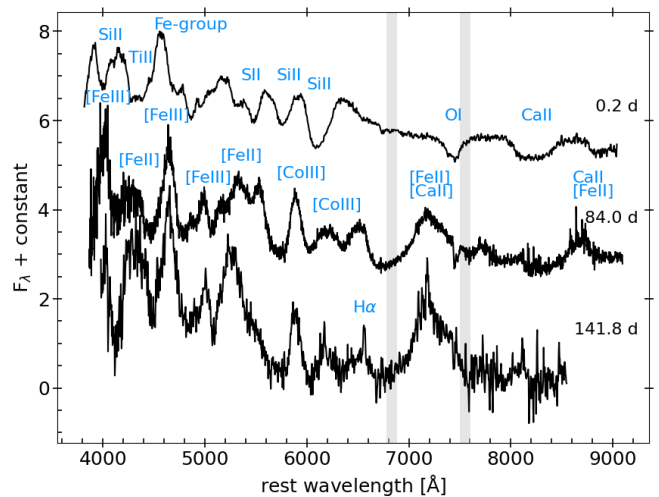


Fig. 3. Optical spectral sequence of SN 2016jaj. All spectra have been corrected by redshift and extinction. The grey columns show the location of the strongest telluric band, which has been removed when possible. The locations of the most prominent spectral features are also indicated. A colour version of this figure can be found in the online journal.

4. Discussion and summary on the nature of SN 2016jae and its progenitor scenario

In the previous sections, we have analyzed the observed properties of SN 2016jae. This supernova, classified as a Type Ia, shows a B-band peak of -17.93 ± 0.11 mag, an intermediate value between that of SN 2011fe (“normal” SN; $M_{B,max} = -19.1$, Ashall et al. 2016) and SN 1991bg (sub-luminous SN prototype; > -17.7 mag, Taubenberger 2017), followed by a fast decrease with Δm_{15} of 1.88 ± 0.10 mag. Despite its early classification as a “normal” SN Ia, the SN observables of SN 2016jae point to a similarity to fast declining and sub-luminous transitional events. The noticeable feature is a narrow H α line that appears in the nebular spectra. This emission line is associated with the SN, and the

¹² For the resolved narrow line components, we first corrected the measured FWHM for the spectral resolution ($width = \sqrt{FWHM^2 - res^2}$) and then computed the velocity ($v = width \times c$).

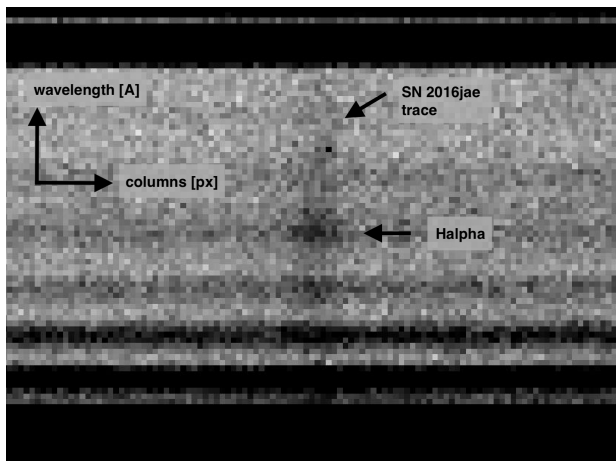


Fig. 4. The H α emission line in the 2D spectrum of SN 2016jae taken with GTC+OSIRIS on 2017 May 18 (phase 141.8 d from the assumed B -maximum date). The wavelength is up and the spatial direction is to the right.

velocities are 650 and 1000 km s⁻¹ at phase 84d and 142d, respectively. The derived FWHM is similar to those obtained for SNe 2018cqj and 2018fhw (~ 1200 km s⁻¹ at 193d and 139d, respectively), the other two low-luminosity SNe Ia with detection of H α emission line in late-time spectra.

Understanding the origin of this H emission can give crucial constraints for the progenitor scenario. We first consider two scenarios: (i) pre-existing CSM material shocked by the SN ejecta, or (ii) in the material stripped by the SN ejecta from an H-rich companion star in a single-degenerate progenitor system.

Nearby CSM can originate from the system before explosion due to the outcome of a common envelope phase. In this case, the expected expansion velocity of H α is of the order of a few hundred km s⁻¹, comparable to that presumed for interacting SNe (e.g. Silverman et al. 2013; Smith 2014). However, the estimated velocities for SNe 2016jae, 2018cqj, and 2018fhw are much higher. Besides, H α should also appear at early phases and accompanied by other Balmer emissions as H β (we noticed the non-detection of H β in SN 2016jae in Section 3.2). In short, it is unlikely that the gas shell was produced by a common envelope phase. Also, the parent stellar population of these three transitional SNe Ia with H α emission was most likely of old age. In fact, both SNe 2018cqj and 2016jae appeared in the outskirts of their putative host galaxies, suggesting either that they are halo objects, whereas the host of SN 2018fhw was a dwarf elliptical. This is consistent with the progenitor environment of the majority of the 91bg-like and transitional SNe (see, e.g., Panther et al. 2019), rather than with that of Type Ia-CSM SNe, which are found in star-forming galaxies (see, e.g., Hamuy et al. 2003; Prieto et al. 2007; Dilday et al. 2012; Silverman et al. 2013).

An alternative is that SN 2016jae exploded in a single degenerate system, and the H material was stripped from the non-degenerate H-rich companion star. It is expected that the stripped material has expansion velocities ≤ 1000 km s⁻¹ (see, e.g., Mattila et al. 2005; Liu et al. 2012) that is consistent with the estimated velocity from the H α line in SN 2016jae. In the recent simulations, Dessart et al. (2020) found that the hydrogen stripped from a non-degenerate companion star can remain undetected at epochs <50d, begin to emerge at 100d and well visible between 150d and 200d (at this time the metal-rich ejecta become increasingly more transparent and faint). This is fully consistent with our observations of SN 2016jae. Besides, these

authors argue that we may expect to see H α and not H β because H α sits in a most transparent regions of the optical range, while H β occurs in a region with strong metal line blanketing. Notice that stripping could also be asymmetrical and the cause of the possible redshift of ~ 200 km s⁻¹ in the H α profile (at both 84d and 142d phases for the adopted $z_{\text{host}} = 0.021$; Prieto et al. 2020; Botyánszki et al. 2018). Actually, Prieto et al. (2020) stressed that the apparent line shift may be related to the uncertainties in the location and redshift of the SN. It may be a concern for SN 2016jae because as discussed in Section 2, it is not clear which galaxy hosts this SN. However, assuming $z_{\text{host}} = 0.019$, the H α peak would be even more blue-shifted by ~ 800 km s⁻¹.

As in SNe 2018cqj and 2018fhw, we can use the luminosity estimation from the nebular spectra and constrain the amount of hydrogen stripped from the non-degenerated companion star. Using the relation introduced by Tucker et al. (2020), which is based on the models of Botyánszki et al. (2018), we can derive a mass of the hydrogen stripped material (M_{st}) of 0.002 M_{\odot} from the two nebular spectra of SN 2016jae. Similarly, following Dessart et al. (2020) and considering the estimated ^{56}Ni mass for SN 2016jae in Section 3.1 (0.15 M_{\odot} ¹³), we obtain a comparable value for M_{st} of 0.003 M_{\odot} . This estimated M_{st} , is similar to that found for SNe 2018cqj and 2018fhw, and as already notice by Dessart et al. (2020), it is much lower than expected ($>0.1 M_{\odot}$) for standard models of SD scenarios for SNe Ia (see, e.g., Marietta et al. 2000; Liu et al. 2012; Botyánszki et al. 2018). We attempted to understand the evolution with time of the H α luminosity considering the measurements for the three SNe with hydrogen detected. As we see in Figure 6, the H α luminosity decreases with the phase of the SN. Dessart et al. (2020) showed that the luminosity of H α accounts for 10% of the radioactive decay energy absorbed by the stripped gas. This dependence implies a connection between the H α luminosity and the characteristic time of the ^{56}Co decay. That is, the luminosity of H α decreases with time, and this is faster when M_{st} is low. The latter is related to the fact that for low M_{st} , γ rays are not efficiently trapped by the stripped material.

To check our estimates of the stripped mass derived from the H α luminosity, we have measured the equivalent width (EQW) of this emission line, which is a parameter that does not depend on the distance or extinction of the object. For this, we have followed the steps described in Dessart et al. (2020) and applied their analytical fit for a DDC25 model. We obtained a M_{st} of 0.014 and 0.066 M_{\odot} at 84d and 142d, respectively, that are consistent with the values derived above.

In conclusion, while the H emission observed in SN 2016jae may be from material stripped from a companion, it seems in conflict with the M_{st} predicted by hydrodynamic models for this type of scenario. Yet, we may consider some mechanism to hide the stripped hydrogen gas. For example, some of the H-rich material may be not visible because it is travelling at higher velocities (although models predict that the amount of this high-velocity material is low; see, e.g., Pan et al. 2012; Liu et al. 2012). Otherwise, the outer layer of the companion star might have been stripped off by an optically dense wind well before the explosion (Hachisu et al. 1999, 2008).

A key characteristic of SN 2016jae is the H α expansion velocity of ~ 1000 km s⁻¹. Such velocity can be reached by opti-

¹³ The value of ^{56}Ni mass allows us to discriminate between the models used by Dessart et al. (2020) for the analytical fit to the correlation between the luminosity of H α and M_{st} . Here we have followed the delayed-detonation model DDC25 with ^{56}Ni mass of 0.12 M_{\odot} .

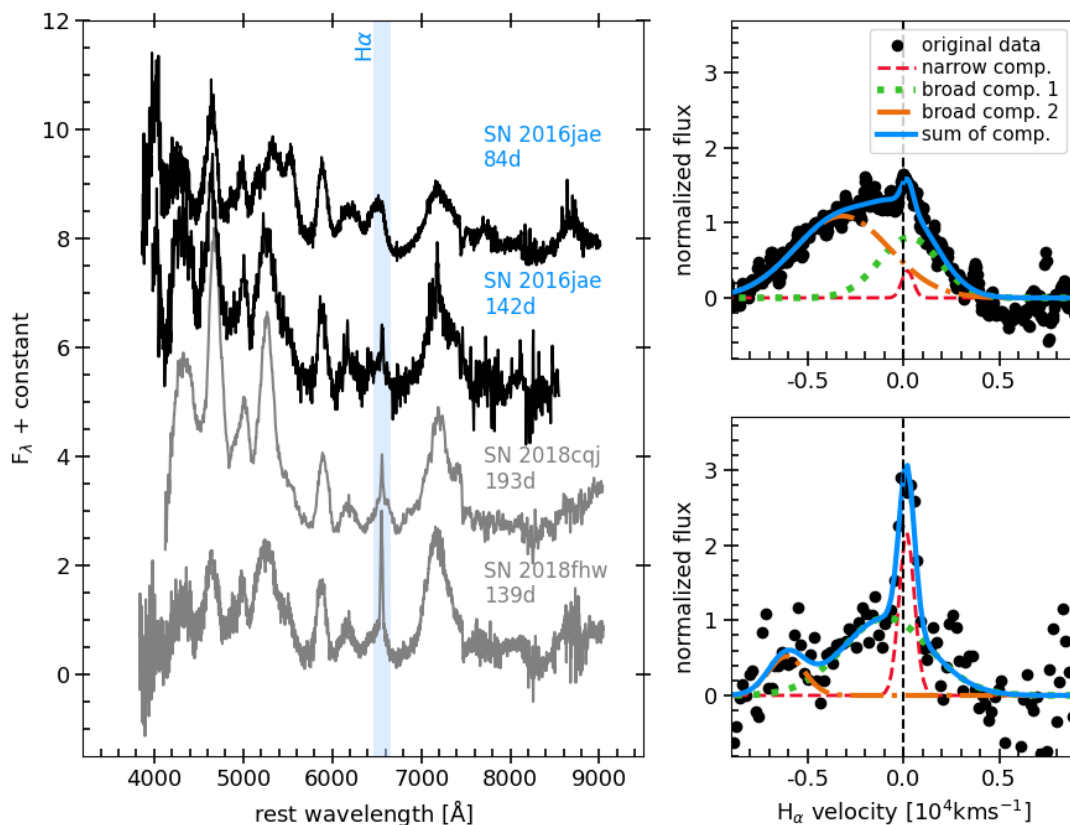


Fig. 5. *Left:* Comparison of SN 2016jae late-time optical spectra, along with those of the SNe 2018cqj and 2018fhw at similar epochs. All spectra have been corrected by redshift and extinction (values adopted from the literature; see also Table B.1). Ages are relative to B maximum light. The locations of the $H\alpha$ emission line is also indicated. *Right:* Decomposition of the $H\alpha$ emission line of SN 2016jae at phases 84.0 (*top*) and 141.8 d (*bottom*). Three Gaussian profiles have been used for the narrow $H\alpha$ and two broad components of iron-group elements.

cally thick winds and nova ejecta (Hachisu et al. 1999; Moriya et al. 2019).

Based on this suggestion, one may consider a binary system made of a WD and a secondary H-rich star which is transferring mass to the WD. When the mass transfer rate becomes larger than the maximum accretion rate for stable H-shell burning on the surface of the WD, the unprocessed material is expelled in the form of an optically thick wind (see, e.g., Wang 2018). If the WD explodes during the wind phase, the resulting SN Ia could show the presence of hydrogen (Hachisu et al. 1999; Kato & Hachisu 2012). Alternatively, the high mass transfer rate may lead to a long series of relatively mild nova eruptions. These nova cycles cause the initial CO WD to grow in mass until it reaches masses of the order of $1.35 - 1.38 M_\odot$ and finally to explode as SN (see, e.g., Hillman et al. 2016 or Hachisu & Kato 2018). This is not the first time that a recurrent nova is proposed as the progenitor of SNe Ia, although this scenario was more often called to explain SNe strongly interacting with the CSM at early times (see, e.g., Dilday et al. 2012; Wood-Vasey & Sokoloski 2006; Hachisu & Kato 2018).

There may be other possibilities that we have not discussed in detail here. For example, as recalled by Dessart et al. (2020), the enclosed ($>0.1 M_\odot$) H-rich material that moves at low velocity may originate from a tertiary star in a triple system or a swept-up giant planet rather than from a non-degenerate companion star (Soker 2019).

Altogether, the observables of SNe 2016jae, 2018cqj, and 2018fhw suggest that these could be transition objects between “normal” SNe Ia and low peak luminosity SNe Ia. The fact that these three supernovae share among the many similarities the presence of H at similar dates is suggestive and raises the possibility of a common progenitor system. Certainly, *the Zorro Diagram*, which includes a large sample of well-observed luminous, “normal” and sub-luminous SNe Ia (Mazzali et al. 2007), suggests that all the SNe considered in this analysis have a similar mass progenitor, consistent with the Chandrasekhar model. However, Dessart et al. (2020) show a better fit of the optical spectrum of SN 2018cqj at 207d after explosion (Prieto et al. 2020) with a mass that is lower than the Chandrasekhar mass. Indeed, there is growing evidence that the properties of low-luminosity supernovae are better explained by sub-Chandrasekhar mass explosion (Stritzinger et al. 2006; Scalzo et al. 2019). At the same time, from a theoretical point of view, it has been ruled out the single degenerate scenario for transitional SNe Ia based on the t_0 - M_{56Ni} relation (Wygoda et al. 2019; Sharon & Kushnir 2020). However, the appearance of hydrogen at nebular phases appears to be not generally expected from the double degenerate scenario and in turn with the sub-Chandrasekhar model for the three SNe of our sample. In short, at the present stage, we cannot link the “coincidence” of these three SNe to a unique evolution scenario or explosion mechanism.

Acknowledgements. N.E.R. thanks D. Kushnir, M. Hernanz and J. Isern for useful discussions and to the telescope’s staff for their excellent support in the ex-

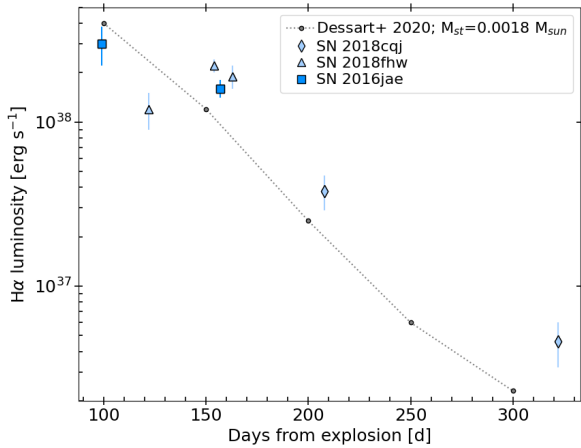


Fig. 6. Evolution of the luminosity of H α of SNe 2016jæ, 2018cqj, 2018fhw. For comparison, we have also plotted an average value for the subset of models with $M_{st} = 0.0018 M_{\odot}$ of Dessart et al. (2020) (dotted line). For the SNe of the sample, we have assumed 15 days of rise-time (average from the values found by Hsiao et al. 2015 and Vallely et al. 2019).

cution of the observations.

N.E.R. and E.C. acknowledges support from MIUR, PRIN 2017 (grant 20179ZF5KS). Support for J.L.P. is provided in part by ANID through the Fondecyt regular grant 1191038 and through the Millennium Science Initiative grant ICN12_009, awarded to The Millennium Institute of Astrophysics, MAS. Based on observations made with the GTC telescope, in the Spanish Observatorio del Roque de los Muchachos of the Instituto de Astrofísica de Canarias, in the island of La Palma. This paper includes data gathered with the 6.5 meter Magellan Telescopes located at Las Campanas Observatory, Chile. We acknowledge ESA Gaia, DPAC and the Photometric Science Alerts Team (<http://gsaweb.ast.cam.ac.uk/alerts>). This work is based (in part) on observations collected at the European Organisation for Astronomical Research in the Southern Hemisphere, Chile as part of PESSTO, (the Public ESO Spectroscopic Survey for Transient Objects Survey) ESO program 188.D-3003, 191.D-0935, 197.D-1075. This research has made use of the NASA/IPAC Extragalactic Database, which is funded by the National Aeronautics and Space Administration and operated by the California Institute of Technology.

References

Ashall, C., Mazzali, P., Sasdelli, M., & Prentice, S. J. 2016, *MNRAS*, 460, 3529
Benetti, S., Cappellaro, E., Mazzali, P. A., et al. 2005, *ApJ*, 623, 1011
Benetti, S., Cappellaro, E., Turatto, M., et al. 2006, *ApJ*, 653, L129
Blondin, S., Dessart, L., & Hillier, D. J. 2015, *MNRAS*, 448, 2766
Blondin, S. & Tonry, J. L. 2007, *ApJ*, 666, 1024
Botyánszki, J., Kasen, D., & Plewa, T. 2018, *ApJ*, 852, L6
Branch, D., Dang, L. C., Hall, N., et al. 2006, *PASP*, 118, 560
Brown, T. M., Baliber, N., Bianco, F. B., et al. 2013, *PASP*, 125, 1031
Burns, C. R., Parent, E., Phillips, M. M., et al. 2018, *ApJ*, 869, 56
Burns, C. R., Stritzinger, M., Phillips, M. M., et al. 2011, *AJ*, 141, 19
Calzetti, D., Kinney, A. L., & Storch-Bergmann, T. 1994, *ApJ*, 429, 582
Chambers, K. C., Magnier, E. A., Metcalfe, N., et al. 2016, *arXiv e-prints*, arXiv:1612.05560
Chen, P., Dong, S., Kochanek, C. S., et al. 2020, *arXiv e-prints*, arXiv:2011.02461
Dessart, L., Leonard, D. C., & Prieto, J. L. 2020, *A&A*, 638, A80
Dilday, B., Howell, D. A., Cenko, S. B., et al. 2012, *Science*, 337, 942
Dong, S., Katz, B., Kollmeier, J. A., et al. 2018, *MNRAS*, 479, L70
Elias-Rosa, N., Pastorello, A., Benetti, S., et al. 2016, *MNRAS*, 463, 3894
Filippenko, A. V., Richmond, M. W., Branch, D., et al. 1992, *AJ*, 104, 1543
Gress, O., Lipunov, V., Buckley, D., et al. 2016, *The Astronomer's Telegram*, 9902, 1
Hachisu, I. & Kato, M. 2018, *ApJS*, 237, 4
Hachisu, I., Kato, M., & Nomoto, K. 1999, *ApJ*, 522, 487
Hachisu, I., Kato, M., & Nomoto, K. 2008, *ApJ*, 679, 1390
Hamuy, M., Phillips, M. M., Suntzeff, N. B., et al. 2003, *Nature*, 424, 651
Hillman, Y., Prialnik, D., Kovetz, A., & Shara, M. M. 2016, *ApJ*, 819, 168

Hodgkin, S. T., Wyrzykowski, L., Blagorodnova, N., & Koposov, S. 2013, *Philosophical Transactions of the Royal Society of London Series A*, 371, 20120239
Hsiao, E. Y., Burns, C. R., Contreras, C., et al. 2015, *A&A*, 578, A9
Kasen, D. 2006, *ApJ*, 649, 939
Kato, M. & Hachisu, I. 2012, *Bulletin of the Astronomical Society of India*, 40, 393
Kinney, A. L., Calzetti, D., Bohlin, R. C., et al. 1996, *ApJ*, 467, 38
Kirshner, R. P., Jeffery, D. J., Leibundgut, B., et al. 1993, *ApJ*, 415, 589
Kollmeier, J. A., Chen, P., Dong, S., et al. 2019, *MNRAS*, 486, 3041
Kriszianas, K., Contreras, C., Burns, C. R., et al. 2017, *AJ*, 154, 211
Leibundgut, B., Kirshner, R. P., Phillips, M. M., et al. 1993, *AJ*, 105, 301
Liu, Z. W., Pakmor, R., Röpke, F. K., et al. 2012, *A&A*, 548, A2
Magnier, E. A., Schlafly, E. F., Finkbeiner, D. P., et al. 2020, *ApJS*, 251, 6
Maguire, K., Sullivan, M., Pan, Y. C., et al. 2014, *MNRAS*, 444, 3258
Maoz, D., Mannucci, F., & Nelemans, G. 2014, *ARA&A*, 52, 107
Marietta, E., Burrows, A., & Fryxell, B. 2000, *ApJS*, 128, 615
Mattila, S., Lundqvist, P., Sollerman, J., et al. 2005, *A&A*, 443, 649
Mazzali, P. A., Chugai, N., Turatto, M., et al. 1997, *MNRAS*, 284, 151
Mazzali, P. A., Röpke, F. K., Benetti, S., & Hillebrandt, W. 2007, *Science*, 315, 825
Moriya, T. J., Liu, D., Wang, B., & Liu, Z.-W. 2019, *MNRAS*, 488, 3949
Nugent, P., Phillips, M., Baron, E., Branch, D., & Hauschildt, P. 1995, *ApJ*, 455, L147
Pan, K.-C., Ricker, P. M., & Taam, R. E. 2012, *ApJ*, 750, 151
Panther, F. H., Seitenzahl, I. R., Ruiter, A. J., et al. 2019, *PASA*, 36, e031
Pereira, R., Thomas, R. C., Aldering, G., et al. 2013, *A&A*, 554, A27
Phillips, M. M. 2012, *PASA*, 29, 434
Phillips, M. M., Lira, P., Suntzeff, N. B., et al. 1999, *AJ*, 118, 1766
Planck Collaboration, Ade, P. A. R., Aghanim, N., et al. 2016, *A&A*, 594, A13
Prieto, J. L., Chen, P., Dong, S., et al. 2020, *ApJ*, 889, 100
Prieto, J. L., Garnavich, P. M., Phillips, M. M., et al. 2007, *arXiv e-prints*, arXiv:0706.4088
Scalzo, R. A., Parent, E., Burns, C., et al. 2019, *MNRAS*, 483, 628
Schlafly, E. F. & Finkbeiner, D. P. 2011, *ApJ*, 737, 103
Sharon, A. & Kushnir, D. 2020, *Research Notes of the American Astronomical Society*, 4, 158
Silverman, J. M., Foley, R. J., Filippenko, A. V., et al. 2012, *MNRAS*, 425, 1789
Silverman, J. M., Nugent, P. E., Gal-Yam, A., et al. 2013, *ApJS*, 207, 3
Smartt, S. J., Valenti, S., Fraser, M., et al. 2015, *A&A*, 579, A40
Smith, K., Cikota, A., Magee, M., Kankare, E., & Yaron, O. 2016a, *Transient Name Server Classification Report*, 2016-1095, 1
Smith, K. W., Cikota, A., Magee, M., et al. 2016b, *The Astronomer's Telegram*, 9908, 1
Smith, K. W., Smartt, S. J., Young, D. R., et al. 2020, *PASP*, 132, 085002
Smith, N. 2014, *ARA&A*, 52, 487
Soker, N. 2019, *Research Notes of the American Astronomical Society*, 3, 153
Stritzinger, M., Burns, C. R., Phillips, M. M., et al. 2010, *AJ*, 140, 2036
Stritzinger, M. & Leibundgut, B. 2005, *A&A*, 431, 423
Stritzinger, M., Leibundgut, B., Walch, S., & Contardo, G. 2006, *A&A*, 450, 241
Taubenberger, S. 2017, *The Extremes of Thermonuclear Supernovae*, ed. A. W. Alsabti & P. Murdin (Springer, Cham), 317
Tonry, J., Denneau, L., Stalder, B., et al. 2016, *Transient Name Server Discovery Report*, 2016-1077, 1
Tonry, J. L., Denneau, L., Heinze, A. N., et al. 2018, *PASP*, 130, 064505
Tucker, M. A., Shappee, B. J., Vallely, P. J., et al. 2020, *MNRAS*, 493, 1044
Turatto, M., Benetti, S., Cappellaro, E., et al. 1996, *MNRAS*, 283, 1
Vallely, P. J., Fausnaugh, M., Jha, S. W., et al. 2019, *MNRAS*, 487, 2372
Wang, B. 2018, *Research in Astronomy and Astrophysics*, 18, 049
Wood-Vasey, W. M. & Sokoloski, J. L. 2006, *ApJ*, 645, L53
Wygodna, N., Elbaz, Y., & Katz, B. 2019, *MNRAS*, 484, 3941
Yaron, O. & Gal-Yam, A. 2012, *PASP*, 124, 668

Appendix A: Additional figures of SN 2016jae.

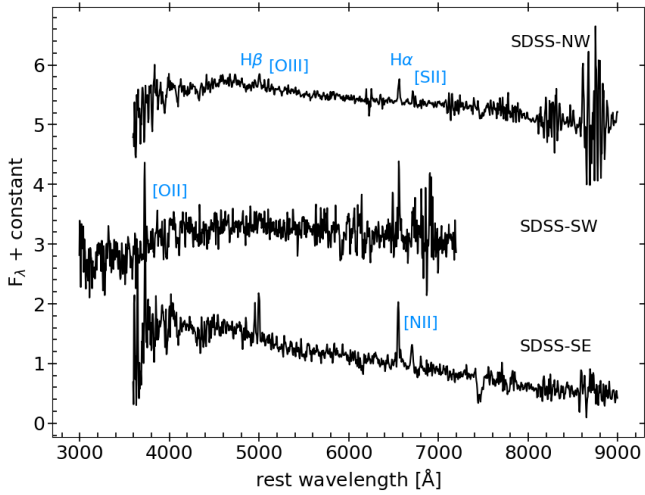


Fig. A.1. Spectra of SDSS-NW, SDSS-SW and SDSS-SE taken with GTC+OSIRIS on 2019 December 3, and 2020 May 10. In particular, the spectrum of SDSS-SW is a combination of the spectra of both epochs. All spectra are in the rest frame and corrected for Galactic extinction.

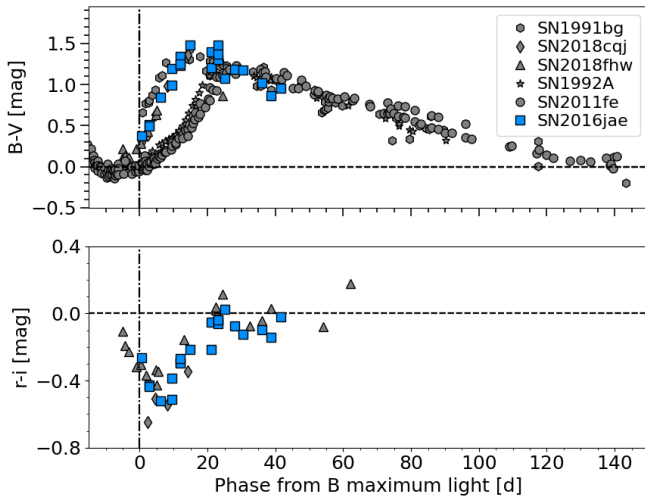


Fig. A.2. Intrinsic colour evolution of SN 2016jae, compared with those of SNe 1991bg, 2018cqj, 2018fhw, 1992A and 2011fe. For both panels, the dot-dashed vertical line indicates the B -band maximum light.

Appendix B: Properties of the supernovae used in this work.

Appendix C: Tables of photometry and spectroscopy of SN 2016jae.

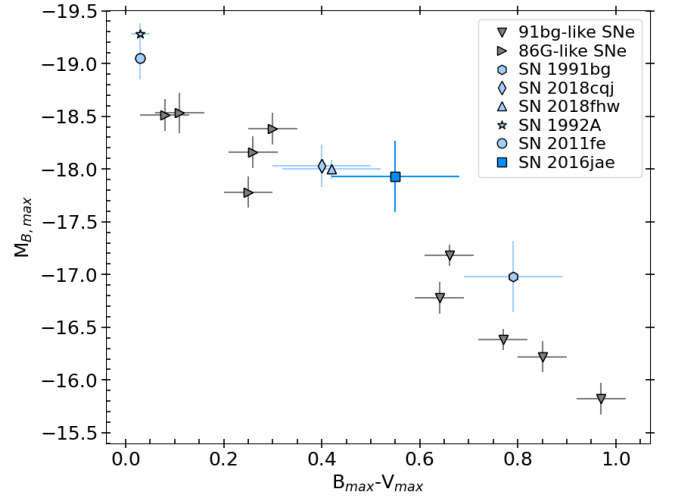


Fig. A.3. $(B_{\max} - V_{\max})$ colour vs. $M_{B,\max}$ of a sample of sub-luminous SNe Ia (91bg-like) and transitional or 86G-like SNe from the Carnegie Supernova Project-I sample of (Krisciunas et al. 2017). The magnitudes were derived using SNooPy light curve fits and the absolute magnitudes were calculated assuming $H_0 = 67.8 \text{ km s}^{-1} \text{ Mpc}$. Magnitudes of SNe 1991bg, 2018cqj, 2018fhw, 1992A, 2011fe and 2016jae are also plotted.

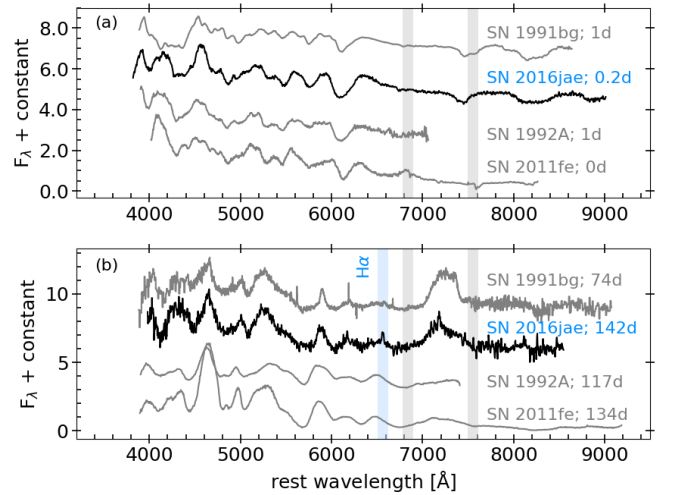


Fig. A.4. Early- ((a)) and late- ((b)) time comparison of SN 2016jae optical spectra, along with those of the sub-luminous SN 1991bg and the “normal” Ia SNe 1992A and 2011fe at similar epochs. All spectra have been corrected by redshift and extinction (adopted values and references are reported in Table B.1). Ages are relative to B maximum light. The grey columns show the location of the strongest telluric band, which has been removed when possible.

Table B.1. Properties of the supernovae used along this work.

SN	Host galaxy	Distance [†] (Mpc)	$E(B - V)_{\text{tot}}$ (mag)	$\sim t_{B,\text{max}}$ (MJD)	Sources
SN 1991bg	NGC 4374	19.1	0.08	48603.2	a
SN 1992A	NGC 1380	22.3	0.01	48640.0	b
SN 2011fe	M101	6.2	0.02	55815.5	c
SN 2018cqj	IC550	78.9	0.03	58294.7	d
SN 2018fhw	2MASX J04180598–6336523	76.2	0.03	58356.8	e
SN 2016jae	?	92.9	0.10	57750.2	This work

[†] Distances have been scaled to $H_0 = 67.8 \text{ km s}^{-1} \text{ Mpc}^{-1}$.

a=Filippenko et al. 1992; Leibundgut et al. 1993; Turatto et al. 1996; b=Phillips et al. 1999; Stritzinger et al. 2010; c=Pereira et al. 2013; Silverman et al. 2012; Maguire et al. 2014; d=Prieto et al. 2020; e=Kollmeier et al. 2019; Vallely et al. 2019.

Table C.1. New r (ABMAG) photometry of SN 2016jae.

Date	MJD	Phase ^a (days)	r (mag)	Instrument key ^b
20161222	57744.28	-5.9	17.39 (0.17)	Gaia
20161230	57752.36	2.2	16.95 (0.15)	Gaia
20170330	57842.98	92.8	20.85 (0.19)	Gaia
20170518	57891.91	141.8	22.53 (0.09)	OSIRIS

^a Phases are relative to B maximum light, MJD = 57750.15 \pm 1.00.

^b Gaia; OSIRIS = 10.4 m Gran Telescopio CANARIAS + OSIRIS located at the Roque de Los Muchachos, Spain

Table C.2. Log of spectroscopy observations of SN 2016jae.

Date	MJD	Phase ^a	Instrumental set-up ^b	Grism or grating	Spectral range (Å)	Resolution ^c (Å)	Seeing (arcsec)	Airmass
20161228	57750.34	0.2	NTT+EFOSC2	gm13+1.00 arcsec	3900-9230	18	1.6	1.32
20170322	57834.19	84.0	Clay/Magellan+LDSS-3	VPH-All+1.00 arcsec	3800-9285	8	1.1	1.67
20170518	57891.91	141.8	GTC+OSIRIS	R500B+1.00 arcsec	4068-8730	7	1.4	1.44

^a Phases are relative to B maximum light, MJD = 57750.15 \pm 1.00.

^b NTT+EFOSC2 = 3.6m New Technology Telescope + EFOSC2 located at the La Silla Observatory, Chile;
Clay/Magellan+LDSS-3 = 6.5m Magellan Clay Telescope + LDSS3 (Low Dispersion Survey Spectrograph 3) located at Las Campanas Observatory, Chile; GTC+OSIRIS = 10.4 m Gran Telescopio CANARIAS + OSIRIS located at the Roque de Los Muchachos, Spain.

^c Measured from the FWHM of the night sky lines.

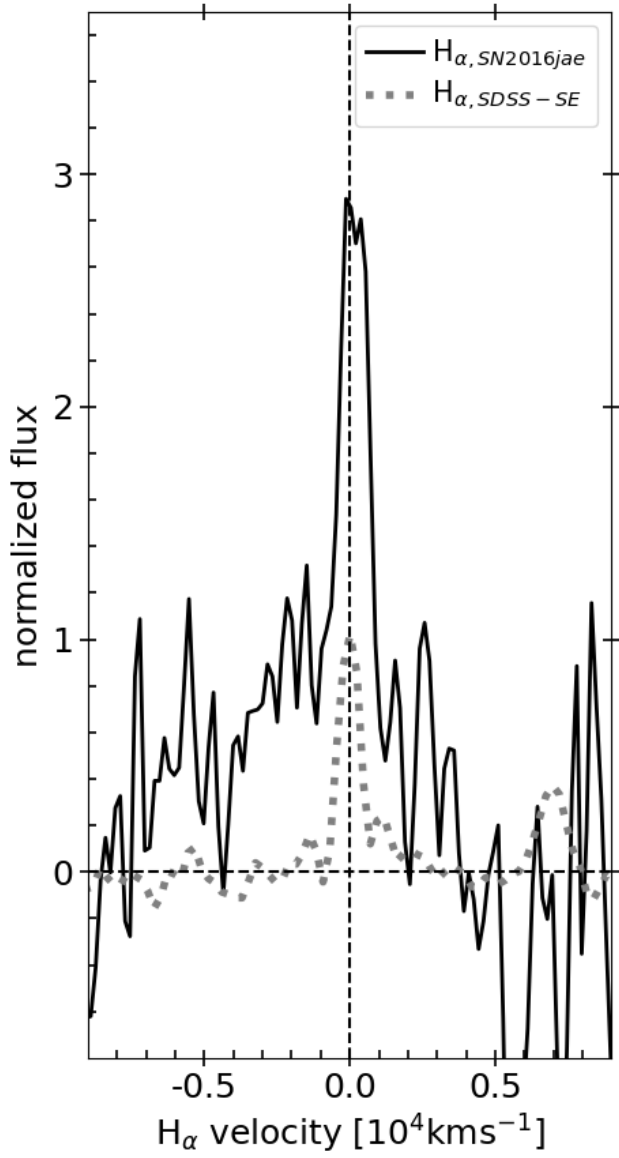


Fig. A.5. $H\alpha$ line profile comparison of SN 2016jae at phase 141.8 d (from the assumed B maximum date) and the spectrum of SDSS-SE (the nearest galaxy with a similar redshift). The dashed lines mark the rest wavelength of $H\alpha$ and the normalized flux = 0.